AIAA 2002-2557

Noise Suppression in Moderate-Speed Multistream Jets

D. Papamoschou
Dept. of Mechanical & Aerospace Engineering
University of California at Irvine
Irvine, CA

8th AIAA/CEAS Aeroacoustics Conference
17-19 June 2002
Breckenridge, Colorado

AIAA-2002-2557

NOISE SUPPRESSION IN MODERATE-SPEED MULTISTREAM JETS

Dimitri Papamoschou *
University of California, Irvine, Irvine, California 92697-3975

This paper presents an exploratory study of alternative jet noise suppression methods for commercial turbofan engines. The basic principle is reduction of the convective Mach number of flow instabilities that produce intense downward-radiated sound. This is possible through a combination of two factors: mixing enhancement of the core stream and thickening of the bypass stream on the underside of the jet. In an initially coaxial jet, these two effects are achieved either by offsetting the nozzles or by deflecting the bypass stream. The latter option, accomplished by installing vanes in the annular exhaust of the bypass flow, proved acoustically superior. Subscale tests of jets approximating the exhaust conditions of CFM56 and JT8D engines showed that, in both cases, the vanes produced significant suppression of downward directed noise. For the CFM56, the peak overall sound pressure level (OASPL) was suppressed by 5 dB and the effective perceived noise level (EPNL) was reduced by 2 dB. For the JT8D, peak OASPL and EPNL were both reduced by 4 dB relative to the ideal fully-mixed exhaust.**

Nomenclature

a	=	speed of sound at jet exit or in freestream
$\overline{a}$	=	speed of sound associated with $\overline{u}$
D	=	diameter
$\dot{m}$	=	mass flow rate
M	=	Mach number at jet exit or in freestream
$\overline{u}$	=	peak mean velocity at given axial location
U	=	velocity at jet exit or in freestream
U_c	=	convective velocity
α	=	geometric angle of attack
γ	=	climb angle
θ	=	polar angle relative to jet centerline
ρ	=	density
ϕ	=	azimuth angle relative to vertical plane

Subscripts

p	=	primary (core) exhaust
s	=	secondary (bypass) exhaust
∞	=	flight conditions

Abbreviations

BPR	=	Bypass Ratio = $\dot{m}_s/\dot{m}_p$
EPNL	=	Effective Perceived Noise Level
OASPL	=	Overall Sound Pressure Level
PNL	=	Perceived Noise Level
SPL	=	Sound Pressure Level

*Professor, Associate Fellow AIAA

** Noise suppression via deflection of the bypass and/or core streams is proprietary to the University of California. U.S. Patent Pending.

Introduction

Aircraft noise is an issue of enormous environmental, financial, and technological impact. There are two main sources of noise in today's commercial aircraft engines: fan/compressor noise and jet noise. Jet noise itself is composed of turbulent mixing noise and, in the case of imperfectly expanded jets, shock noise [1]. Turbulent mixing is by far the biggest problem and is extremely difficult to control. The most celebrated formula for turbulent mixing noise is the scaling law

$$\overline{p'^2} \sim U_j^n \tag{1}$$

It comes from dimensional analysis of the solution to Lighthill's acoustic analogy [2, 3]. The left hand side is the sound intensity, U_j is the jet velocity, and $n = 8$ for low-speed jets and approaches 3 for very-high-speed jets. This formula is the cornerstone of

jet noise reduction efforts over the last half-century: reduction of jet speed using exhaust mixers or by increasing the engine bypass ratio.

Turbulent mixing is governed by the velocity difference across the mixing region, rather than by the absolute velocity. A more complete version of Eq. 1, therefore, should be

$$\overline{p'^2} \sim (U_j - U_\infty)^n \qquad (2)$$

where U_∞ is the velocity of the medium surrounding the jet flow. This formula must be used with caution. It is valid only for *shear-layer-type* mixing between the jet and the surrounding medium. It does not apply to *wake-type* mixing that occurs in the vicinity of the nozzle due to the finite thicknesses of the nozzle lip and of the exit boundary layers. In fact, wake-generated noise will worsen with increasing U_∞. Experiments on hot jets in forward flight [4] confirm the validity of Eq. 2 for noise radiating in the rear arc, which is produced by large turbulent eddies. Noise emitted laterally or in the forward arc, generated mainly from fine-scale turbulence, was not attenuated by the flight effect. The reasons for the lack of attenuation are not clear and have been the subject of debate; it is possible this type of noise is influenced by wake effects near the nozzle exit. Figure 1 shows a representative plot of the directivity of OASPL for a hot jet in static and flight conditions [4]. The reduction in peak OASPL is substantial, about 6 decibels.

In coaxial jets, as created by separate-flow turbofan engines, the primary (core) jet is initially surrounded by the secondary (bypass) stream which acts as a moving medium. Given that the velocity ratio of these two flows is typically $U_s/U_p = 0.7$, one would expect dramatic reductions in the noise emitted by the core stream. As will be shown later, this is not the case. In the coaxial exhaust of typical engines, the secondary stream becomes fully mixed well upstream of the end of the primary potential core. As a result, a substantial part of the core noise source region is not covered by the secondary flow. Some noise reduction certainly occurs, but not near the levels one would have expected from Eq. 2.

Equation 2 nevertheless offers a strong incentive to explore alternative methods for noise reduction. Is it possible to reduce the *relative* velocity in the noise-emitting region of the core jet, while maintaining the same absolute core velocity? In other words, can we create a "forward-flight effect" without a huge secondary flow? In an aircraft engine, the exhaust velocities, Mach numbers, and mass flow rates are largely fixed by the engine cycle – one has little freedom in altering them. What can change, however, is the nozzle configuration. Recent work on dual-stream, high-speed jets has shown that substantial noise reduction is achievable by reshaping the nozzle from coaxial to eccentric [5]. Downward-directed Mach wave emission was reduced by the combination of two factors: (a) shortening of the primary potential core (relative to the coaxial case); and (b) thickening of the secondary flow in the downward direction [6]. The resulting synergism allowed the secondary stream to "shield" effectively the noise source region of the primary jet. In broader terms, these experiments suggest that, in a dual-stream jet, shaping of exhaust flow away from traditional configurations has the potential for significant noise reduction.

Questions remain, however, regarding the physical mechanisms and general use of this approach. Why was the primary potential core shortened? Does this technique extend to lower-speed jets where Mach wave radiation is not as intense? And, are there alternatives to the eccentric arrangement? These issues are addressed here through a combination of empirical modeling and exploratory experimentals. First, the concept of "relative velocity" is quantified better in terms of the convective Mach number M_c of the flow instability. Second, preliminary models are constructed for the axial distribution of M_c. Third, experiments on a variety of nozzle configurations clarify important physical mechanisms and identify promising configurations for noise reduction. The study then applies those configurations to subscale tests simulating the exhaust conditions of two widely-used engines, the General Electric CFM56 and the Pratt & Whitney JT8D. The experiments were conducted in UCI's Jet Aeroacoustics Facility (Fig. 2) which has been described extensively in prior publications [5, 7]. All sound measurements presented here are in the acoustic far field. Estimates of perceived noise level (PNL) use the flight path shown in Fig. 3. Details on the PNL estimation can be found in Ref. [7].

Convective Mach Number M_c

The large-scale turbulent structures of the jet shear layers can be viewed, at a conceptual level, as instability waves traveling with a convective speed U_c. Letting $\eta(x,t)$ represent the vortex sheet between the jet and a quiescent ambient, the simplest wave

representation is of the form

$$\eta(x,t) \;=\; Ae^{i(x-U_c t)} \tag{3}$$

where a wavenumber of unity has been chosen for simplicity. With the amplitude A constant, the instability radiates sound to the far field when the convective Mach number

$$M_c \;=\; \frac{U_c}{a_\infty} > 1 \tag{4}$$

The next level of realism is to consider the non-parallel (growing) nature of the mean flow. In that case, linear stability theory shows that a disturbance at fixed frequency amplifies and then decays with axial distance. Instead of a simple wave, we are now dealing with a wave packet

$$\eta(x,t) \;=\; A(x)e^{i(x-U_c t)} \tag{5}$$

As has been shown by numerous past investigations[1, 8, 9, 10], the amplitude modulation $A(x)$ changes dramatically the sound radiated by the instability. This is readily apparent when writing $\eta(x,t)$ in Fourier space,

$$\eta(x,t) \;= \frac{1}{2\pi}\int_{-\infty}^{\infty} \hat{A}(k-1)e^{ik\left(x-\frac{U_c}{k}\right)}dk \tag{6}$$

The wave packet is a superposition of individual simple waves each with wavenunber k, amplitude $\hat{A}(k-1)dk/(2\pi)$, and phase speed U_c/k. The phase Mach number of each individual wave is

$$m_c \;=\; \frac{U_c/k}{a_\infty} \;=\; \frac{M_c}{k} \tag{7}$$

Figure 4 plots m_c versus k for $M_c = 0.5$. Also plotted is a sketch of a generic $\hat{A}(k-1)$. Instabilities with $|k| < M_c$ are supersonic and radiate to the far field; those with $|k| > M_c$ are subsonic and decay exponentially with distance away from the jet axis. The energy contained in the radiating sound field is governed by the integral of $\hat{A}(k-1)$ from $-M_c$ to M_c. This example shows that subsonic instability waves can radiate sound to the far field if they are amplitude modulated. One can view this as a form of Mach wave radiation, although it is much weaker than its supersonic counterpart. Nevertheless, Mach waves carry sound to the far field so this source of noise can be very important in moderate-speed jets.

Clearly, as M_c declines there is less energy contained in the radiated sound field. This motivates the noise reduction approach presented here. Is it possible to reduce M_c at constant exit flow conditions? The following sections address this question.

Effect of Nozzle Geometry on $M_c(x)$

A large number of experiments confirm that most of the large-scale turbulent mixing noise comes from the region around the end of the potential core [11, 12, 13, 14]. Any scheme to reduce noise via reduction of the convective Mach number M_c must take this fact into account. This leads to a more specific definition of the noise reduction approach proposed here: *make M_c at the end of the potential core as low subsonic as possible.*

In a jet with fixed exit flow conditions, reduction of M_c entails one or both of the following basic methods: (a) controlling U_c; (b) controlling the medium surrounding the instability wave. The former requires some form of excitation that can change U_c not only at the nozzle exit but five to twenty diameters downstream, depending on the length of the potential core. There is no experimental evidence that this is possible in realistic flows. The latter scheme is more plausible as it involves manipulation of a secondary stream. Today all commercial aircraft engines have a secondary stream - the bypass flow.

In a dual-stream jet, there are two convective Mach numbers that influence noise emission: one for the primary instability with respect to the secondary stream,

$$M_{c_p}(x) \;=\; \frac{U_{c_p}(x) - \overline{u}_s(x)}{\overline{a}_s(x)} \tag{8}$$

and the other for the secondary instability with respect to the ambient,

$$M_{c_s}(x) \;=\; \frac{U_{c_s}(x) - U_\infty}{a_\infty} \tag{9}$$

In non-axisymmetric arrangements there is also an azimuthal dependence of the mean flow variables. Which one of the two convective Mach numbers is more important depends on the volume and intensity of noise sources associated with each distribution. For low secondary mass flow rate (low bypass ratio) M_{c_p} is expected to govern noise emission. For very large secondary mass flow rates M_{c_s} could become equally or more important. As will be shown next, in coaxial engine exhausts the primary (core) flow has a much longer potential core that does the secondary (bypass) flow. The end of the potential core is associated with very strong turbulent fluctuations. It is possible, therefore, that M_{c_p} is influential even for large bypass ratios. For this reason, more weight is given here on M_{c_p} than on M_{c_s}.

Direct measurements of turbulent structure convection in jets and shear layers [15, 16], coupled with surveys of the mean flow in coaxial and eccentric jets [6], offer preliminary empirical tools for the prediction of $M_{c_p}(x)$ and $M_{c_s}(x)$. This prediction should be viewed as more qualitative than quantitative as it is based on limited number of data and on models whose accuracy is on the order of 10%. However, it is expected to capture fundamental trends needed to illustrate the philosophy of the approach. Appendices A and B summarize the models.

Figure 5 shows predictions of $M_{c_p}(x)$ and $M_{c_s}(x)$ in a static jet with CFM56 exit conditions (Table 1). The convective Mach number of the core jet alone, plotted in Fig. 5a, is 0.85 at the jet exit and starts declining where the potential core ends, x/D_p=5.5. For the coaxial jet, Fig. 5b, M_{c_p} drops to 0.18 at the jet exit but starts rising past the end of the secondary potential core and reaches a maximum of 0.45 at the end of the primary potential core, x/D_p=16. Note the dramatic elongation of the primary core with addition of the annular bypass flow. Offsetting the nozzles to an eccentric geometry, Fig. 5c, shortens the primary core to x/D_p=9 and doubles the length of the secondary core on the underside of the jet. As a result, M_{c_p} on the underside of the jet never exceeds 0.22. The eccentric jet, therefore, is expected to be quieter in the downward direction than the coaxial jet.

It is important to realize that static conditions are not representative of the conditions under which noise from an airplane is monitored. Forward flight has significant influence on the distribution of convective Mach numbers, particularly on $M_{c_s}(x)$. For this reason, Figure 6 plots the M_c distributions for the CFM56 case with $M_\infty = 0.3$. Compared to the static case, M_{c_s} is reduced from 0.6 to 0.35. This should translate into a very substantial reduction of noise emitted by the bypass flow. Offsetting the nozzles reduces the peak value of $M_{c_p}(x)$ from 0.38 to 0.20. Given that the secondary flow is now much quieter, offsetting the nozzles may produce a stronger benefit at forward flight than at static conditions.

Figure 7 shows convective Mach number predictions for a lower-bypass engine, the JT8D-219 (Table 2). This is a mixed-flow engine that potentially could be modified to a separate-flow configuration. The peak M_{c_p}s of the perfectly-mixed exhaust and of the coaxial exhaust are roughly the same, around 0.9. Offsetting the nozzles reduces the peak M_{c_p} to 0.6.

Past experiments [5, 7], and those presented later in this paper, confirm that the eccentric exhaust is quieter than the coaxial exhaust. See Figs. 8a and 8b for the generic coaxial and eccentric nozzle shapes. As mentioned earlier, a key mechanism is the shortening of the potential core (mixing enhancement) of the primary flow. Enhanced mixing was thought to be caused by exposure of part of the primary stream to the ambient, hence creation of a larger velocity differential across the shear layer on the upper side of the jet.

This motivated a potential refinement to the eccentric nozzle, the arcuate nozzle shown in Fig. 8c. It was designed to have a very smooth transition from a full annulus at the nozzle entrance to 2/3 (240-deg.) annulus at the nozzle exit. The flow lines at the nozzle exit were parallel. The arcuate nozzle was tested against coaxial and eccentric nozzles having the same primary and secondary exit cross sectional areas.

Figure 9 shows far-field spectra of sound from jets issued from coaxial, eccentric, and arcuate nozzles. All exit flow conditions were identical. While the eccentric nozzle reduced noise, the arcuate nozzle produced negligible noise reduction at low frequencies and very small reduction at high frequency. It became evident that the eccentric nozzle creates effects not present in the arcuate nozzle and that the aforementioned reason for enhanced mixing was wrong or incomplete. Although this development was initially disappointing, it shed some light on the fluid mechanics of the eccentric nozzle and spawned alternative configurations that probably would not have been considered otherwise.

The failure of the parallel-flow, arcuate nozzle to reduce noise suggests strongly that the eccentric nozzle produces flow deflections that help promote mixing of the primary flow. A speculative drawing of the streamline shapes exiting the eccentric nozzle is presented in Fig. 10. A stagnation region is formed at the closed portion of the meniscus-shaped secondary flow passage. Streamlines in that region deflect to exit the nozzle and create locally skewed mixing layers between the primary and secondary flows. Past theoretical and experimental studies have shown that increasing the skew angle can result in very significant increase in mixing [17, 18].

Deflection of Bypass Stream

The last observation triggered investigation of methods to control the mixing layer skew angle and simultaneously deflect the bypass stream. It was also desired to maintain the overall configuration coaxial, simplifying the task of potentially implementing these methods on aircraft engines. This section overviews two such configurations. The first one involved placing a wedge in the annular bypass nozzle, essentially creating an arcuate nozzle but with nonparallel flow in the vicinity of the wedge. The second one involved installation of vanes in the bypass stream to deflect the bypass flow downward.

The wedge configuration is shown in Fig. 11. Experimentation with a variety of wedge shapes and sizes showed that the wedge angle was the most critical parameter. At the same base dimension, wedges with large angles reduced downward-emitted noise appreciably while those with small angle produced little reduction. This finding is in accord with the negligible noise reduction produced by the arcuate nozzle (Fig. 8c). Figure 12 compares spectra produced by a clean coaxial nozzle, a coaxial nozzle with wedge inserted in the bypass flow, and an eccentric nozzle. In the direction of peak noise emission, the wedge and the eccentricity produced roughly the same acoustic benefit. It appears, therefore, that streamline deflection is a critical aspect of noise reduction. In other polar directions, the wedge nozzle was moderately inferior to the eccentric one. As a result, the overall noise benefit of the wedge configuration (in terms of OASPL and PNL) was somewhat smaller than that of the eccentric nozzle. This observation is based on a limited number of experiments so one should be careful not to generalize prematurely. The wedge configuration in fact produces substantial reduction in the peak sideline noise (at azimuth angles up to 90°), a feature that will be exploited in future studies.

Figure 13 shows an exemplary drawing of the approach using vanes in the exhaust of the bypass stream. It is believed that this deflection scheme achieves two goals simultaneously: create skewed mixing layers in the vicinity of the nozzle exit and direct most of the bypass stream to the lower side of the jet so that it shields the end of the potential core. Figure 14 shows spark schlieren images that tend to support this hypothesis. The clean coaxial jet spreads very slowly. Insertion of vanes enhances mixing considerably and thickens the bypass stream on the underside of the jet. The deflectors produced superior noise reduction compared to the wedge and eccentricity methods. Applied to an engine, they could be actively deflected or deployed, confining any thrust losses to the takeoff and landing segments only. The next section concentrates on experiments using this approach.

Subscale Simulation of Two Engines

Subscale jet experiments, using helium-air mixtures, simulated the exhaust conditions of two engines: the General Electric CFM56 and the Pratt & Whitney JT8D-219. See Fig. 2 for an overview of the experimental setup. Both engines produce static thrust in the 20,000-lb class. Estimates of perceived noise level assumed a flight path (Fig. 3) with a takeoff roll of 1300 m followed by a straight climb at $\gamma = 12°$ and at a geometric angle of attack $\alpha = 6°$. The experiments compared the acoustics of the following exhaust configurations: clean coaxial; coaxial with deflectors; eccentric; and, in the case of the JT8D, fully-mixed. Tables 1 and 2 summarize the flow conditions, nozzle configurations,and aerodynamic force predictions for each simulated engine.

Figure 15 shows a picture of the CFM56 nozzle with deflectors attached. The core nozzle had a plug that approximated the configuration of this engine found on many aircraft. The outer wall of the core nozzle extended past the exit of the bypass nozzle. Four vanes, made of thin metal sheet, were attached on the outer wall of the core nozzle immediately past the exit of the bypass nozzle. With $\phi = 0$ indicating the downward vertical direction, the vanes were placed at azimuth angles $\phi = \pm 70°$ and $\pm 110°$. The vane angle of attack was approximately 10°. The size of each vane was 4 mm in chord by 3 mm in width. The width was slightly smaller than the annulus thickness of the bypass duct.

The forces on the vanes were calculated from basic aerodynamic relations [19]. Each vane was treated as a wing with aspect ratio equal to twice the width divided by the chord length. The two-dimensional lift slope was assumed to be 0.1/deg and the parasite drag coefficient was assumed to be 0.01. Because of the small aspect ratio, the three-dimensional lift slope is quite small (around 0.04 /deg), allowing deflections up to about 25° without exceeding a lift coefficient of 1.0. It is expected, therefore, that the vanes are not stalled even at such high geometric angle of attack.

Figure 16 shows spectra in the direction of peak emission for the CFM56 cases. In the low- to mid-frequency range, the eccentric nozzle reduced the SPL by 3 dB and the nozzle with vanes reduced the SPL by 5 dB. Figure 17 shows the directivity of OASPL. There is significant reduction of OASPL at the shallow angles. The maximum level of OASPL was reduced by 3 dB in the eccentric case and by 5 dB in the vane case. For higher angles, CFM56-ECC displays a moderate noise increase while CFM56-4V10e practically coincides with the coaxial clean case. The advantage of CFM56-4V10e is also evident in the PNL comparison of Fig. 18. The effective perceived noise level (EPNL) was reduced by 2.0 dB in CFM56-4V10e versus 0.6 dB in CFM56-ECC.

The nozzle of the JT8D-2V20i configuration is pictured in Fig. 19. Here the bypass duct extended past the end of the core duct. Two vanes were installed inside the bypass duct immediately downstream of the lip of the core nozzle. The vanes were installed at $\phi = \pm 90^\circ$ and at an angle of attack of 20°. Their dimensions were 3 mm in width by 4 mm in chord. The width was about 95% of the bypass annulus thickness, so the vanes did not intrude into the core stream. Figure 20 compares the peak-emission spectra of JT8D-COAX, JT8D-ECC, and JT8D-2V20i. Both the eccentricity and the vanes reduce noise significantly, but the vanes are clearly superior. At the moderate frequency range of 200-500 Hz (full-scale), the vanes produced a 3-4 dB benefit relative to the eccentric nozzle. Noise in the upward direction was roughly equal to that of clean coaxial exhaust, as shown in Fig. 21. This is different from the eccentric case in which upward-directed noise matches that of the isolated core jet, which is considerably louder than the coaxial jet [5]. The fact that the jet does not get much noisier in the upward direction should mitigate concerns about intense upward-directed sound reflecting from aircraft surfaces or atmospheric gradients towards the ground.

Comparisons of OASPL, plotted in Fig. 22, include the above cases and the fully-mixed exhaust. The vanes produce the largest reduction in peak OASPL. Both the eccentric exhaust and the exhaust with vanes are quieter than the mixed-flow exhaust. In terms of perceived noise, the exhaust with vanes is again superior, as shown in the PNL time history of Fig. 23. EPNL was reduced by 5.5 dB relative to the coaxial case and by 3.8 dB relative to the mixed-flow case. Note that, in this experiment, the mixed-flow exhaust is idealized. The actual mixed-flow exhaust has non-uniformities and carries noise form the internal mixer. The benefit of the separate-flow exhaust with vanes, relative to the mixed exhaust, is thus expected to be better than that shown here.

Practical Implementation Issues

Application of bypass deflectors to an aircraft engine is conceptually straight-forward as it does not involve major changes in the powerplant design. In fact, for an initially mixed-flow engine like the JT8D this method might bring simplicity by getting rid of the internal mixer. The vanes could be rotated to a certain angle of attack during the noise-sensitive segments of flight and placed at zero angle otherwise. This will confine thrust losses to the takeoff/landing phases only. Alternatively, the vanes could be deployed during takeoff/landing and then stowed flush with the nacelle surface, creating an even cleaner flow path. If a small thrust loss, on the order of one percent or less, can be tolerated for the entire mission of the airplane, the deflectors could be fixed, thereby simplifying nacelle design.

Placement of deflectors outside the bypass duct (Fig. 15) should not impact the engine cycle are as the deflectors would not change the effective cross-sectional area of the bypass nozzle. If the deflectors are placed inside the bypass duct, some adjustment to the engine cycle may be required. It is in fact possible to use the vanes both for deflecting the bypass stream and for controlling the exit area of the bypass nozzle. The latter may help reduce broadband shock noise that occurs at cruise when the bypass stream is underexpanded.

For an aircraft with wing-mounted engines, the lift force on the vanes (which for the current experiments is estimated at 3-5% of engine thrust) should have negligible impact on longitudinal trim as the axial location of the engines is near the axial location of the center of gravity. In a configuration with rear-mounted engines, vane lift will have a small effect on trim. An approximate analysis of longitudinal stability for a DC9/MD80-type airplane shows that a vane lift equal to 5% of engine thrust can be counteracted with one degree of stabilizer trim or 3° of elevator deflection.

Concluding Remarks

The OASPL plots of Figs. 1, 17, and 22 bear a resemblance which is not believed to be coincidental.

The combination of skewed mixing and concentration of the bypass stream to the underside of the jet appears to produce a "forward flight effect" in addition to the one that occurs naturally in a coaxial jet. More precisely, based on the preliminary empirical models described earlier in the paper, the aforementioned methods reduce the convective Mach numbers of instabilities that cause downward-radiated noise. Of the configurations examined so far, the vanes in the bypass duct are superior to the other configurations in reducing downward noise. As mentioned earlier, the wedge configuration (Fig. 11) shows good potential for reducing sideline noise. The vane and wedge arrangements should be seen as specific embodiments of a general approach for deflecting the bypass stream sideward and downward while maintaining an coaxial exhaust structure.

The examples shown in this paper are two of several deflector arrangements that have been tried in the recent past. All of them reduce noise when used in the spirit of Fig. 13. The investigation to date has not been very systematic and the vane design and installation have been rather crude. What is clear from the experiments is that the results are quite sensitive on the placement and geometry of the vanes. There is great potential, therefore, for optimization and improvements through a systematic study of a large parameter space that includes deflector geometry, deflector placement, and nozzle geometry. This should be accompanied by a thorough investigation of the flow physics of each configuration.

Special Notice

Acknowledgments

The support by NASA Glenn Research Center is gratefully acknowledged (Grant NAG-3-2345 monitored by Dr. Khairul B. Zaman). Ms. Erin Abbey is thanked for her work on nozzle design.

Appendix A: Mean Flow Relations

This section presents a summary of relations for predicting basic features of the mean flow field of dual-stream jets. For further details the reader should consult Ref. [6]. The relations use the "classical" formula for the growth rate of a fully-turbulent, planar shear layer,

$$\delta'(\mathcal{R},\mathcal{S},M_{c,\mathrm{sym}}) = 0.14\frac{(1-\mathcal{R})(1+\sqrt{\mathcal{S}})}{1+\mathcal{R}\sqrt{\mathcal{S}}}\times \left[0.23+0.77\exp(-3.5M_{c,\mathrm{sym}}^2)\right] \tag{10}$$

where $\mathcal{R}$ is the velocity ratio, $\mathcal{S}$ is the density ratio, and $M_{c,\mathrm{sym}}$ is the symmetric convective Mach number. For coaxial jets, the basic idea is that the length of the primary potential core core, $L_{p,\mathrm{COAX}}$, lies somewhere between the potential core length of the single jet, L_{SINGLE}, and the potential core length of the coflowing jet, $L_{\mathrm{COFLOWING}}$, by an amount dependent on the length of the secondary potential core, $L_{s,\mathrm{COAX}}$. For the single jet,

$$\frac{L_{\mathrm{SINGLE}}}{D_p} = \left\{\delta'\left(0,\frac{\rho_\infty}{\rho_p},\frac{U_p}{a_p+a_\infty}\right)\right\}^{-1} \tag{11}$$

For the coflowing jet (a jet submerged in a very large secondary flow),

$$\frac{L_{\mathrm{COFLOWING}}}{D_p} = \left\{\delta'\left(\frac{U_s}{U_p},\frac{\rho_s}{\rho_p},\frac{U_p+U_s}{a_p+a_s}\right)\right\}^{-1} \tag{12}$$

The length of the secondary potential core is

$$\frac{L_{s,\mathrm{COAX}}}{D_p} = 2.8\frac{H}{D_p}\left[\frac{L_{\mathrm{COFLOWING}}/D_p}{\delta'_s L_{\mathrm{COFLOWING}}/D_p+1}\right] \tag{13}$$

where

$$\delta'_s = \delta'\left(\frac{U_\infty}{U_p},\frac{\rho_\infty}{\rho_s},\frac{U_s-U_\infty}{a_s+a_\infty}\right) \tag{14}$$

and H is the exit thickness of the secondary stream.

The length of the primary core of the coaxial jet is

$$\frac{L_{p,\mathrm{COAX}}}{L_{\mathrm{SINGLE}}} = 1+\tanh\left(2.8\frac{L_{s,\mathrm{COAX}}}{L_{\mathrm{COFLOWING}}}\right)\times \left(\frac{L_{\mathrm{COFLOWING}}-L_{\mathrm{SINGLE}}}{L_{\mathrm{SINGLE}}}\right) \tag{15}$$

For the eccentric jet, the length of the primary core is

$$L_{p,\mathrm{ECC}} = L_{\mathrm{SINGLE}}+0.3(L_{p,\mathrm{COAX}} - L_{\mathrm{SINGLE}}) \tag{16}$$

and the length of the secondary core on the underside of the jet is

$$L_{s,\mathrm{ECC}} = 2L_{s,\mathrm{COAX}} \tag{17}$$

For both coaxial and eccentric cases, the peak mean velocity $\overline{u}(x)$ past the end of the primary potential core decays according to

$$\frac{d(U_p/\overline{u}_p)}{d(x/D_m)} = 0.1 \tag{18}$$

where

$$D_m \;=\; D_p\sqrt{1+\mathrm{BPR}} \tag{19}$$

is the mass-flow-rate equivalent diameter. The peak mean velocity of the secondary stream past the end of the secondary potential core decays according to

$$\frac{d(U_s/\overline{u}_s)}{d(x/H)} = 0.1 \tag{20}$$

Equations 10-20 allow evaluation of the axial distributions of the peak mean velocity for the primary and secondary flows. The corresponding values of speed of sound and Mach number are obtained by assuming that the mean total temperature obeys the Crocco-Busemann relation

$$\overline{T}_0(x) = \frac{\overline{T}_{0_2}\overline{u}_1 - \overline{T}_{0_1}\overline{u}_2}{\overline{u}_1 - \overline{u}_2} + \frac{\overline{T}_{0_1} - \overline{T}_{0_2}}{\overline{u}_1 - \overline{u}_2}\overline{u}(x) \tag{21}$$

where subscripts 1 and 2 represent the end conditions of each axial distribution.

Appendix B: Convective Mach number

Prediction of the convective Mach number is based on the empirical formulae proposed by Murakami & Papamoschou [16]. Considering a shear layer between a fast stream (1) and a slow stream (2), the convective Mach number of eddies relative to the slow stream is

$$M_c = M_{c,\mathrm{sym}} + \frac{d}{\sqrt{1+(\overline{a}_2/\overline{a}_1)^2}} \tag{22}$$

where

$$M_{c,\mathrm{sym}} = \frac{\overline{u}_1 - \overline{u}_2}{\overline{a}_1 + \overline{a}_2}, \tag{23}$$

and

$$d \;=\; \begin{cases} 1.25\ln M_{c,\mathrm{sym}} + 1.11 & , M_{c,\mathrm{sym}} > 0.41 \\ 0 & , M_{c,\mathrm{sym}} \le 0.41 \end{cases} \tag{24}$$

References

[1] Tam, C.K.W., and Chen, P., "Turbulent Mixing Noise from Supersonic Jets," *AIAA Journal*, Vol. 32, No. 9, 1994, pp. 1774-1780.

[2] Lighthill, M.J., "On Sound Generated Aerodynamically: I. General Theory" *Proceedings of the Royal Society of London Series A*," Vol. 211, 1952, pp. 564-581.

[3] Lighthill, M.J., "On Sound Generated Aerodynamically: II. Turbulence as a Source of Sound," *Proceedings of the Royal Society of London Series A*," Vol. 222, 1954, pp. 1-32.

[4] Hoch, R.G. and Berthelot, M., "Use of the Bertin Aerotrain for the Investigation of Flight Effects on Aircraft Engine Exhaust Noise," *Journal of Sound and Vibration,* Vol. 54, No. 2, 1977, pp. 153-172.

[5] Papamoschou, D. and Debiasi, M., "Directional Suppression of Noise from a High-Speed Jet," *AIAA Journal*, Vol. 39, No. 3, 2001, pp. 380-387.

[6] Murakami, E., and Papamoschou, D. "Mean Flow Development of Dual-Stream Compressible Jets," *AIAA Journal*, Vol. 40, No. 6, 2002, pp. 1131-1138.

[7] Papamoschou, D. and Debiasi, M., "Mach Wave Elimination Appied to Turbofan Engines," AIAA-2002-0368.

[8] Crighton, D.G. and Huerre, P., "Shear-Layer Pressure Fluctuations and Superdirective Acoustic Sources," *Journal of Fluid Mechanics*, Vol. 220, 1990, pp. 355-368.

[9] Avital, E.J., Sandham, N.D, and Luo, K.H., "Mach Wave Radiation in Mixing Layers. Part I: Analysis of the Sound Field," *Theoretical and Computational Fluid Dynamics*, Vol. 12, 1998, pp. 73-90.

[10] Tam, C.K.W., "Jet Noise: Since 1952," *Theoretical and Computational Fluid Dynamics,*" Vol. 10, 1998, pp. 393-405.

[11] Panda, J. and Zaman, K.B.M.Q., "Density Fluctuation in Asymmetric Nozzle Plumes and Correlation with Far Field Noise," AIAA-2001-0378.

[12] Panda J. and Seasholtz, R.G. "Experimental Investigation of Density Fluctuations in High-Speed Jets and Correlation with Generated Noise *Journal of Fluid Mechanics,* vol.450, Jan. 2002, pp.97-130.

[13] Hileman, J. and Samimy, M. "Turbulence Structures and the Acoustic Far Field of a Mach 1.3 Jet," *AIAA Journal*, Vol.39, No.9, 2001, pp.1716-27.

[14] Narayanan, S., Barber, T.J., and Polak, D.R., "High Subsonic Jet Experiments: Turbulence and Noise Generation Studies," *AIAA Journal*, Vol. 40, No. 3, 2002, pp. 430-437.

[15] Papamoschou, D. and Bunyajitradulya, A.,"Evolution of Large Eddies in Compressible Shear Layers," *Physics of Fluids*, Vol. 9, No. 3, 1997, pp. 756-765.

[16] Murakami, E. and Papamoschou, D., "Eddy Convection in Supersonic Coaxial Jets," *AIAA Journal*, Vol. 38, No.4, 2000, pp. 628-635.

[17] Ganyu, L. and Lele, S.K. "Inviscid Instability of Skewed Compressible Mixing Layer, " *Journal of Fluid Mechanics,* Vol. 249, 1993, pp. 441-463.

[18] Fric, T.E., "Skewed Shear-Layer Mixing Within a Duct," *AIAA Journal*, Vol.34, No.4, 1996, pp.847-9.

[19] Shevell, R.S., "Fundamentals of Flight," Prentice Hall, 1989.

Table 1: CFM56 Cases (BPR=4.8)

Test	Configuration	D_p^* (mm)	U_p (m/s)	M_p	D_s (mm)	U_s (m/s)	M_s	F_x^{**}	F_y^{**}
CFM56-BASE	Coaxial (clean)	10.0	480	0.90	23.4	330	0.96	0.0%	0.0%
CFM56-ECC	Eccentric	10.0	480	0.90	23.4	330	0.96	Unknown	Unknown
CFM56-4V10e	Coaxial with four vanes inclined 10°, ext. to bypass duct	10.0	480	0.90	23.4	330	0.96	0.8%	3.8%

* This is the effective (area-based) diameter of the primary nozzle. Actual dimensions are 14.4 mm ID with a 10-mm plug.

* F_x and F_y are estimates of the axial and transverse forces, respectively, caused by the nozzle modifications. They are presented in percent of total thrust.

Table 2: JT8D-219 Cases (BPR=1.7)

Test	Configuration	D_p (mm)	U_p (m/s)	M_p	D_s (mm)	U_s (m/s)	M_s	F_x^{**}	F_y^{**}
JT8D-COAX	Coaxial (clean)	14.4	580	1.06	21.6	370	1.05	0.0%	0.0%
JT8D-MIX	Fully mixed	14.4	460	1.05	-	-	-	0.0%	0.0%
JT8D-ECC	Eccentric	14.4	580	1.06	21.6	370	1.05	Unknown	Unknown
JT8D-2V20i	Coaxial with two vanes inclined 20°, int. to bypass duct	14.4	580	1.06	21.6	370	1.05	1.3%	5.0%

** F_x and F_y are estimates of the axial and transverse forces, respectively, caused by the nozzle modifications. They are presented in percent of total thrust.

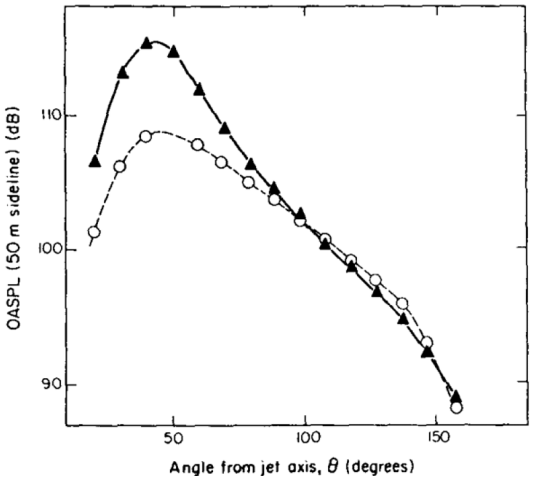

Fig.1 Overall sound pressure level versus emission angle for a single jet at static conditions (solid symbols) and in forward flight (open symbols). Jet Mach number was near sonic, jet speed was 550 m/s, and flight speed was 82 m/s. From Ref. [4].

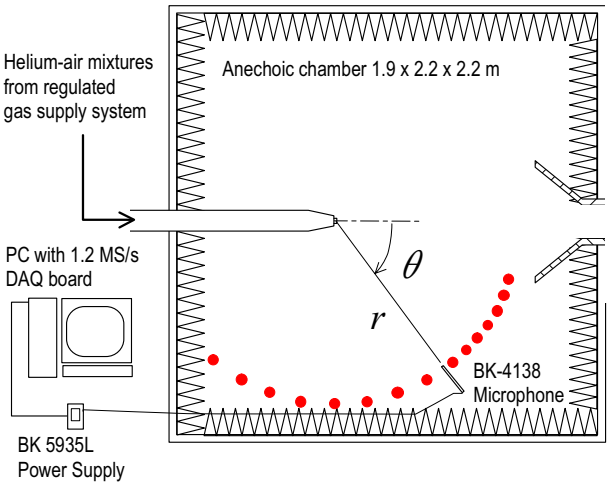

Fig.2 UCI Jet Aeroacouctics Facility.

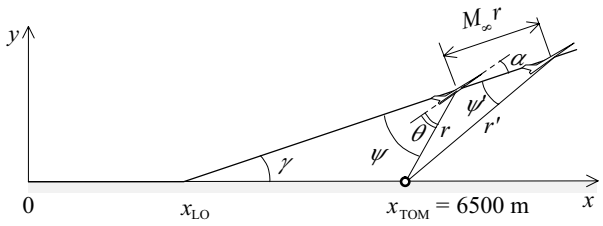

Fig.3 Flight path used for estimating perceived noise level.

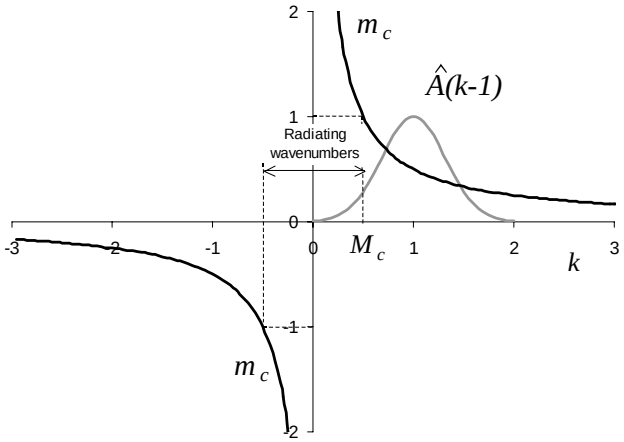

Fig.4 Phase Mach number versus wavenumber for $M_c = 0.5$.

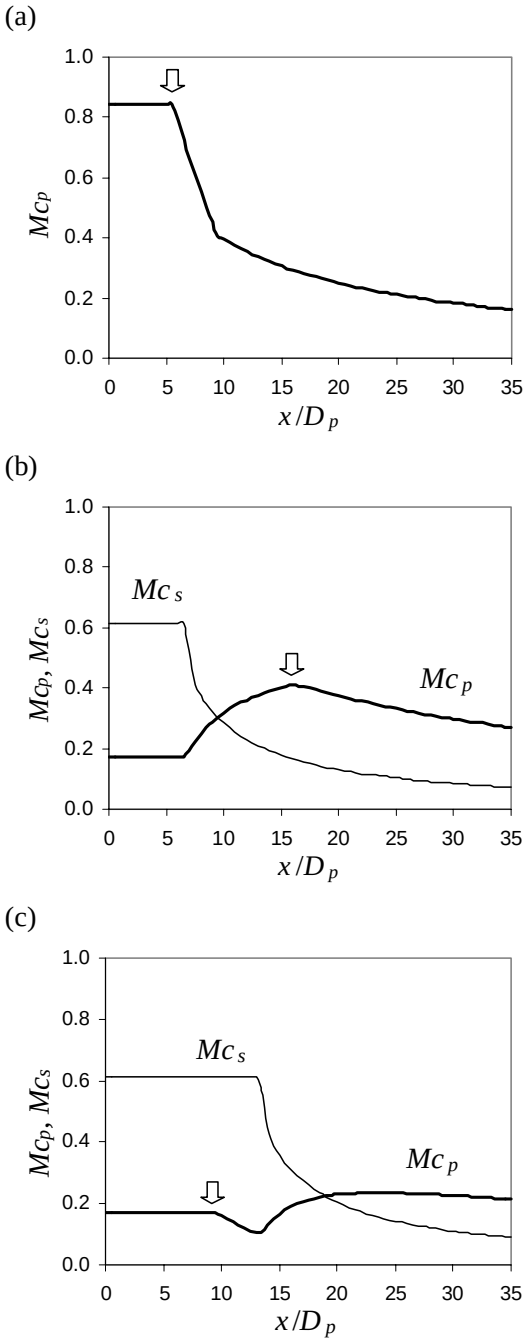

Fig.5 Estimates of convective Mach number distributions for the CFM56 exit flow at static conditions. (a) Core stream alone; (b) coaxial exhaust; (c) underside of eccentric exhaust. Arrow indicates end of primary potential core.

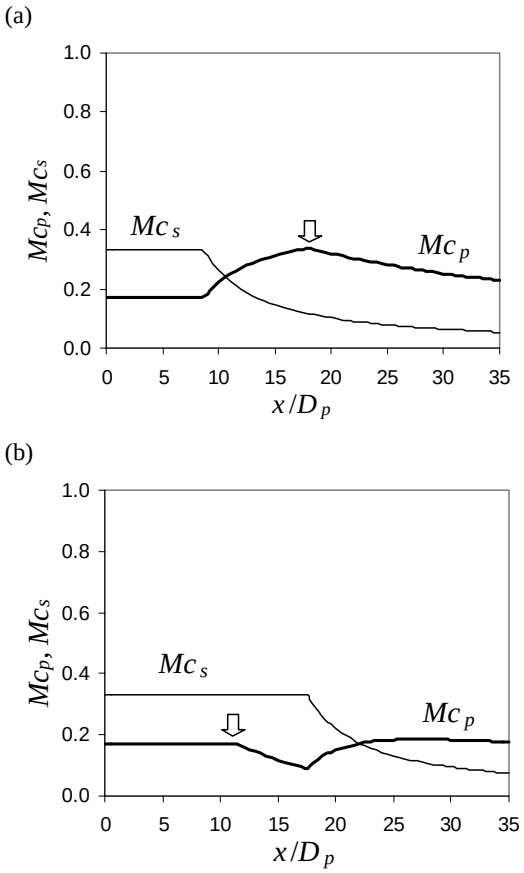

Fig.6 Estimates of convective Mach number distributions for the CFM56 exit flow in forward flight ($M_\infty = 0.3$). (a) Coaxial exhaust; (b) underside of eccentric exhaust. Arrow indicates end of primary potential core.

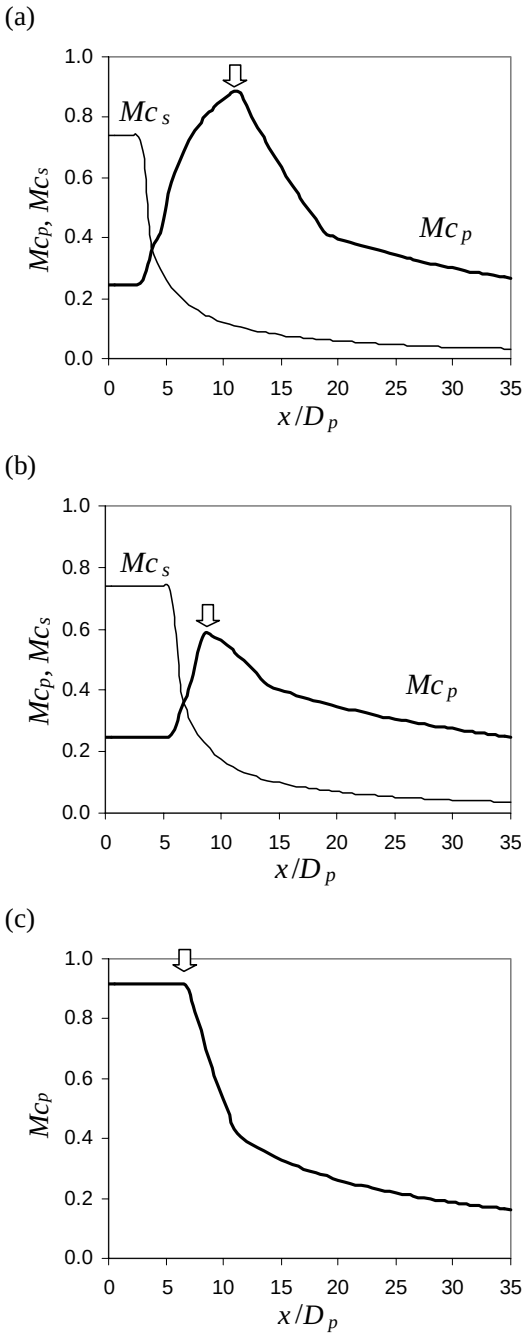

Fig.7 Estimates of convective Mach number distributions for the JT8D exit flow at static conditions. (a) Coaxial exhaust; (b) underside of eccentric exhaust; (c) fully-mixed exhaust. Arrow indicates end of primary potential core.

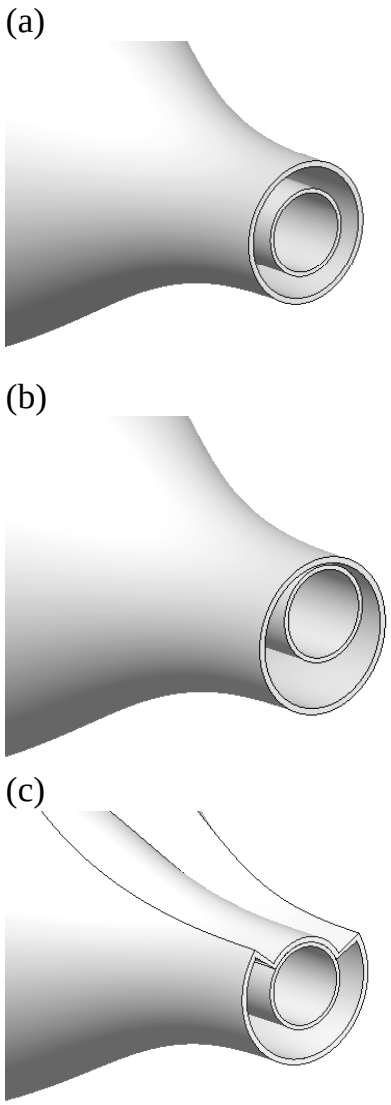

Fig.8 Exhaust geometry of (a) coaxial; (b) eccentric; and (c) arcuate nozzles.

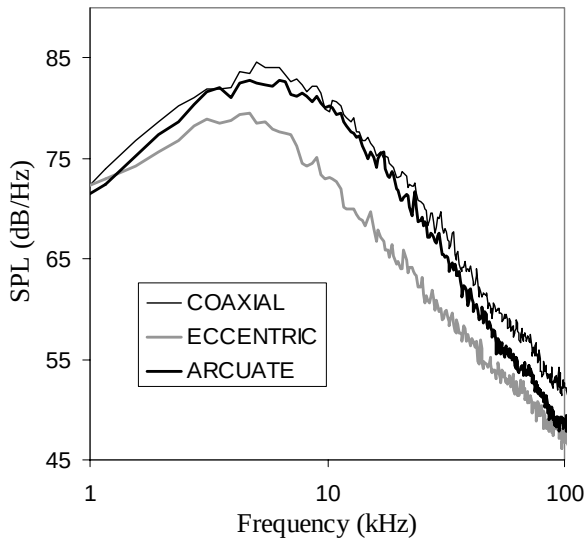

Fig.9 Spectra in the downward direction of peak emission for coaxial, eccentric, and arcuate nozzles. $U_p = 600$ m/s, U_s=360 m/s, and BPR=2.5.

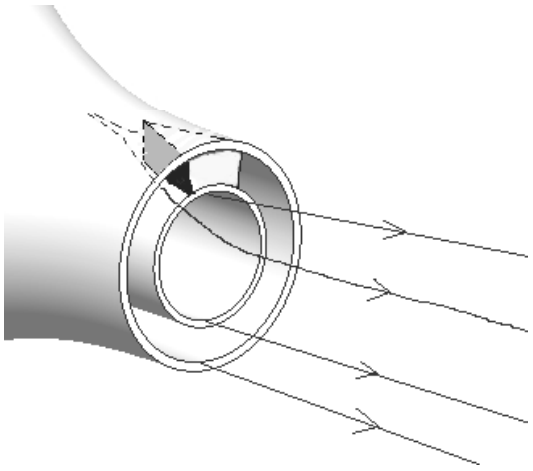

Fig.11 Coaxial nozzle with wedge inserted in the bypass annulus.

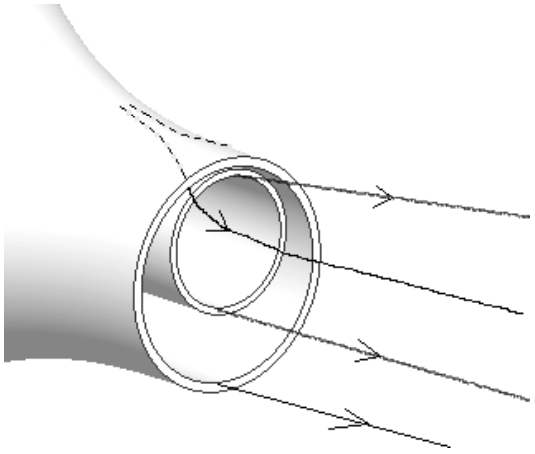

Fig.10 Conjecture on the streamline paths in the eccentric nozzle exhaust.

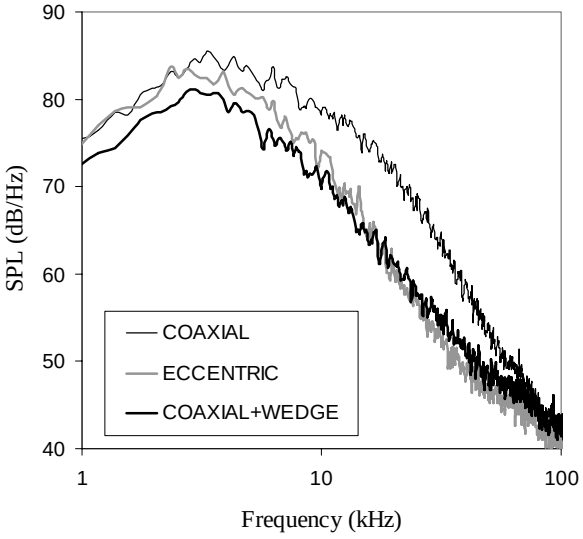

Fig.12 Spectra in the downward direction of peak emission for jets issuing from coaxial, coaxial with wedge, and eccentric nozzles. $U_p = 520$ m/s, U_s=330 m/s, and BPR=2.5.

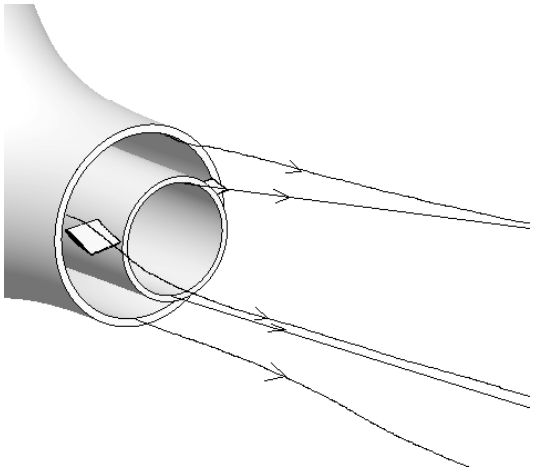

Fig.13 Coaxial nozzle with deflector vanes installed in the bypass exhaust.

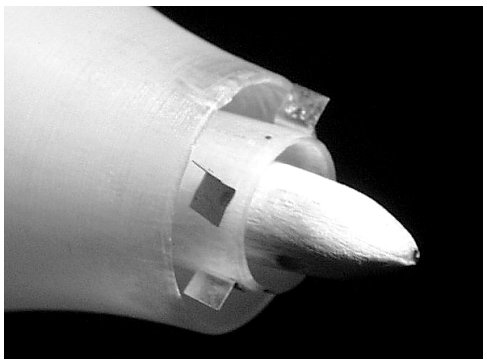

Fig.15 Picture of CFM56-4V10e nozzle.

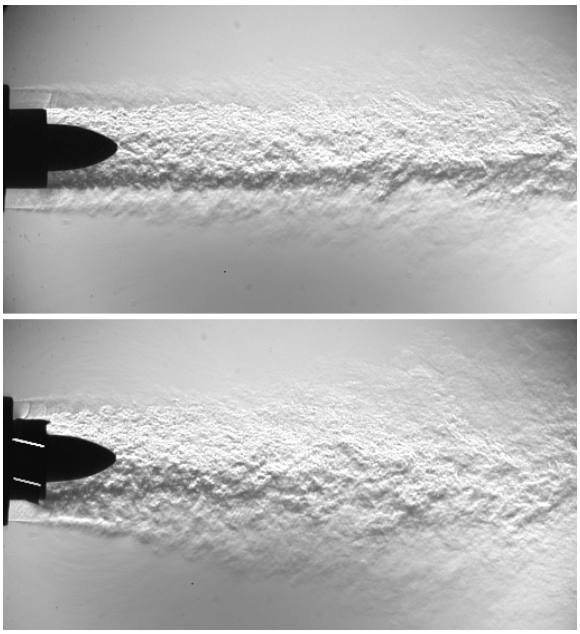

Fig.14 Schlieren images of CFM56 exhaust flow. Upper: clean coaxial nozzle. Lower: coaxial nozzle with four vanes installed immediately downstream of the bypass duct.

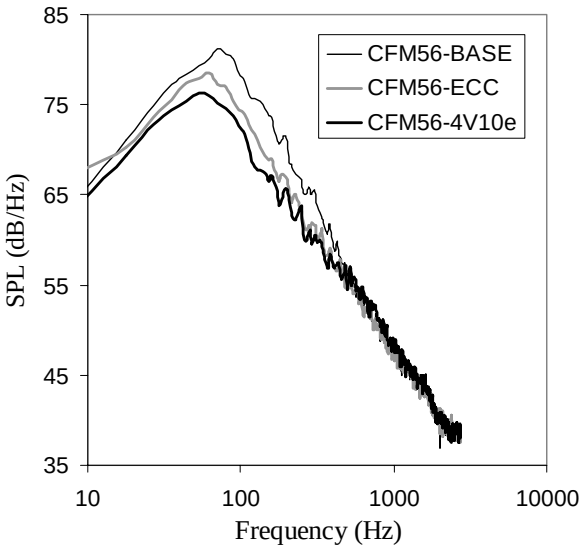

Fig.16 Spectra in the downward direction of peak emission, $\theta = 25°$, for the CFM56 coaxial, eccentric and vane configurations. The spectra were scale-up to full-size engine.

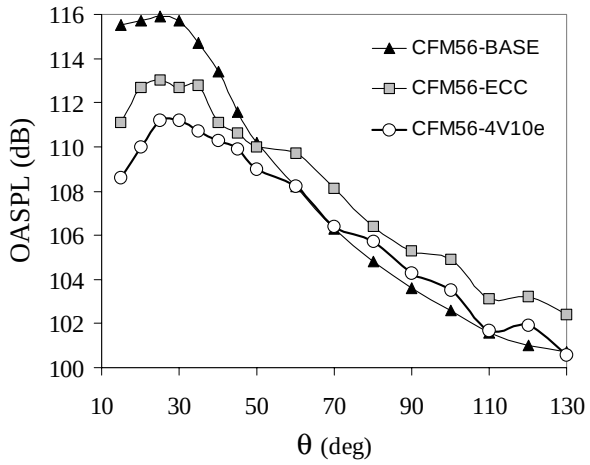

Fig.17 Downward directivity of OASPL for the CFM56 cases.

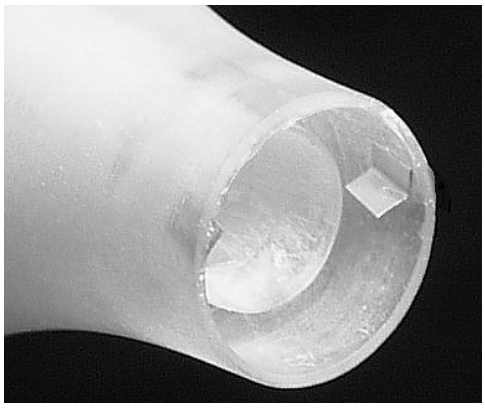

Fig.19 Picture of JT8D-2V20i nozzle.

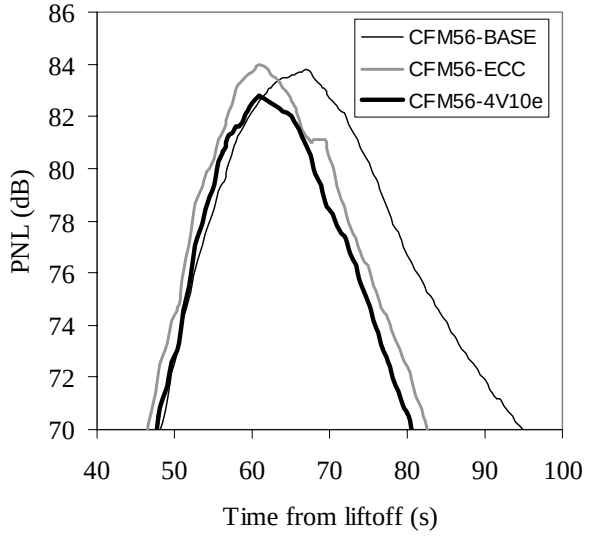

Fig.18 Time history of PNL for the CFM56 cases. EPNL (dB): 86.2 for BASE; 85.4 for ECC; and 84.2 for 4V10e.

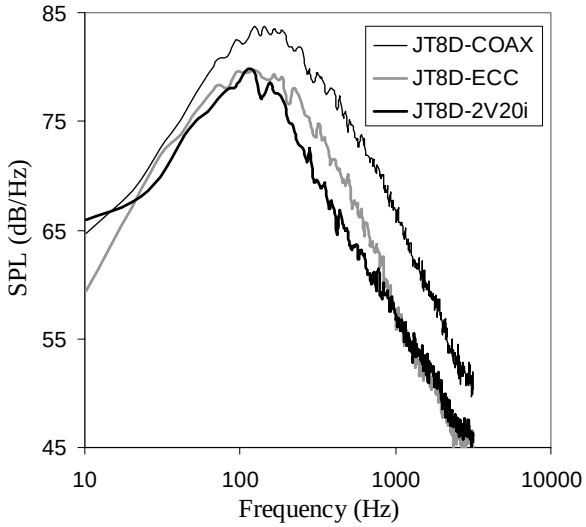

Fig.20 Spectra in the downward direction of peak emission, $\theta = 40°$, for the JT8D coaxial, eccentric, and vane configurations. The spectra were scale-up to full-size engine.

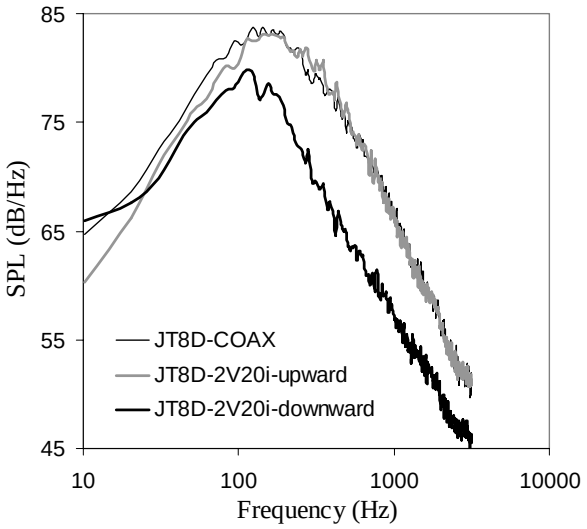

Fig.21 Spectra in the upward and downward directions of peak emission for the JT8D coaxial and vane configurations. The spectra were scale-up to full-size engine.

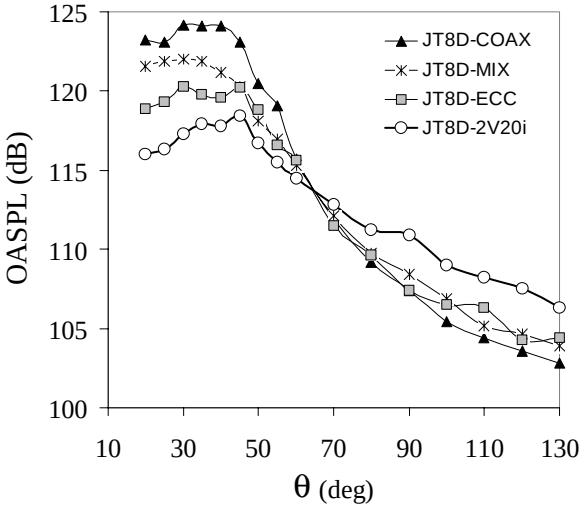

Fig.22 Downward directivity of OASPL for the JT8D cases.

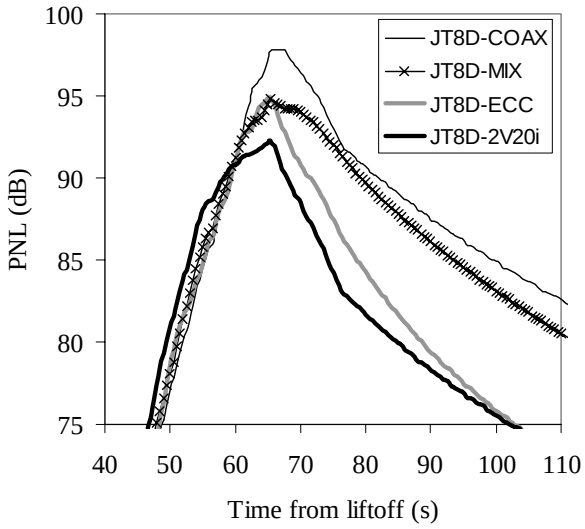

Fig.23 Time history of PNL for the JT8D cases. EPNL (dB): 98.9 for COAX; 97.2 for MIX; 94.9 for ECC; and 93.4 for 2V20i.